

# An Analysis of the Three Material Beam

ELTON G. ENDEBROCK and RALPH M. RICHARD

Respectively, Assistant Professor of Civil Engineering, New Mexico State University, and Associate Professor of Civil Engineering, University of Arizona

A plane stress elasticity solution to the simply supported, three material beam is developed. Results are obtained for beams whose dimensions and material properties simulate composite beams consisting of two materials bonded together by a third material. It is shown that the elementary formulas for stresses and deflections yield sufficiently accurate values under certain conditions. In addition, slip, a quantity often measured in experimental work, is influenced by many factors, and therefore is generally not reliable for use in interpreting test results. Experimental results are presented to verify the effectiveness of the mathematical solution.

•IN recent years considerable research has been conducted on beams composed of two or more materials. Most of this research has been concerned with the behavior of composite beams for use in highway and building construction (1). Composite beams usually consist of a steel beam and a concrete slab joined either by mechanical connectors, or recently, by epoxy resins (2, 3). Many experimental studies of composite beams have been conducted and several mathematical solutions have been developed (4, 5, 6). Through experimental studies and mathematical analyses, the conditions under which the elementary formulas for stresses and deflections are sufficiently accurate have been determined for composite beams utilizing spaced mechanical connectors; however, these conditions may not apply to composite beams having a continuous connection between the slab and beam even though some of the solutions for beams with spaced mechanical connectors were based on the assumption that the connection was continuous. Also, the existing mathematical solutions have not compared favorably with all experimental results, i. e., in the case of slips. Because of these uncertainties and discrepancies, a more exact mathematical solution is desirable.

## THEORETICAL DEVELOPMENT

The model beam consists of three material layers or individual beams of different depths and having different material properties (Fig. 1). The mathematical expressions describing the behavior of the three material, simply supported beam are obtained by employing the methods of the theory of elasticity. A plane stress condition is assumed; hence, determination of the solution consists of generating a stress function that satisfies the biharmonic equation of elasticity and the appropriate boundary conditions. A stress function is determined for each material layer, and the normal and shearing stresses and the displacements at the interface of the adjoining layers are equated.

The stress function  $\phi$  for each material layer is assumed in the form

$$\phi = f(y) \sin \frac{n\pi x}{L} \quad (1a)$$

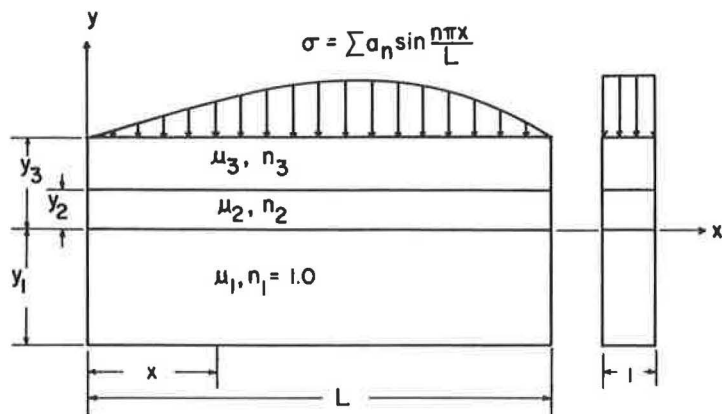


Figure 1. Mathematical model.

where  $f(y)$  is a function of  $y$  only,  $L$  is the length of the beam, and  $n$  is an integer. Substitution of  $\phi$  into the biharmonic equation yields an ordinary linear differential equation in  $f(y)$  which has a solution

$$f(y) = C_1 \cosh \alpha y + C_2 \sinh \alpha y + C_3 y \cosh \alpha y + C_4 y \sinh \alpha y \quad (1b)$$

where  $C_1$ ,  $C_2$ ,  $C_3$ , and  $C_4$  are constants of integration, and  $\alpha = n\pi/L$ .

The normal stresses  $\sigma_x$  and  $\sigma_y$  and the shearing stress  $\tau_{xy}$  are obtained from the stress function  $\phi$ . They are

$$\sigma_x = \frac{\partial^2 \phi}{\partial y^2} = \sin \alpha x [C_1 \alpha^2 \cosh \alpha y + C_2 \alpha^2 \sinh \alpha y + C_3 \alpha (2 \sinh \alpha y + \alpha y \cosh \alpha y) + C_4 (2 \cosh \alpha y + \alpha y \sinh \alpha y)] \quad (2a)$$

$$\sigma_y = \frac{\partial^2 \phi}{\partial x^2} = -\alpha^2 \sin \alpha x [C_1 \cosh \alpha y + C_2 \sinh \alpha y + C_3 y \cosh \alpha y + C_4 y \sinh \alpha y] \quad (2b)$$

$$\tau_{xy} = -\frac{\partial^2 \phi}{\partial x \partial y} = -\cos \alpha x [C_1 \alpha \sinh \alpha y + C_2 \alpha \cosh \alpha y + C_3 (\cosh \alpha y + \alpha y \sinh \alpha y) + C_4 (\sinh \alpha y + \alpha y \cosh \alpha y)] \quad (2c)$$

The stress functions for all three material layers have the same form as Eq. 1; however, they differ because the constants of integration are not the same for each layer. The horizontal displacement  $u$  and the vertical displacement  $v$  enter into the boundary conditions; hence, it is required that they be obtained. The relationships between the strains, displacements, and stresses are

$$\epsilon_x = \frac{\partial u}{\partial x} = \frac{1}{E} (\sigma_x - \mu \sigma_y) \quad (3a)$$

$$\epsilon_y = \frac{\partial v}{\partial y} = \frac{1}{E} (\sigma_y - \mu \sigma_x) \quad (3b)$$

$$\gamma_{xy} = \frac{\partial v}{\partial x} + \frac{\partial u}{\partial y} = \frac{2(1+\mu)}{E} \tau_{xy} \quad (3c)$$

where  $E$  is the modulus of elasticity and  $\mu$  is Poisson's ratio.

The stress equations (Eq. 2) are substituted into the strain equation (Eq. 3). Eqs. 3a and 3b are integrated to obtain the displacements  $u$  and  $v$ . Integration of these equations yields two arbitrary functions which are evaluated by substituting the displacements  $u$  and  $v$  into Eq. 3c. The resulting expressions for  $u$  and  $v$  are

$$\begin{aligned} u = & -\frac{\cos \alpha x}{E} \{C_1 \alpha (1+\mu) \cosh \alpha y + C_2 \alpha (1+\mu) \sinh \alpha y + C_3 [2 \sinh \alpha y \\ & + \alpha y (1+\mu) \cosh \alpha y] + C_4 [2 \cosh \alpha y + \alpha y (1+\mu) \sinh \alpha y]\} \\ & + Ay + B \end{aligned} \quad (4a)$$

$$\begin{aligned} v = & -\frac{\sin \alpha x}{E} \{C_1 \alpha (1+\mu) \sinh \alpha y + C_2 \alpha (1+\mu) \cosh \alpha y + C_3 [\alpha y (1+\mu) \sinh \alpha y \\ & + (-1+\mu) \cosh \alpha y] + C_4 [\alpha y (1+\mu) \cosh \alpha y + (-1+\mu) \sinh \alpha y]\} \\ & - Ax + F \end{aligned} \quad (4b)$$

where  $A$ ,  $B$ , and  $F$  are constants of integration. These constants are associated with rigid body motions, and are taken equal to zero here.

The constants of integration are then evaluated from the boundary conditions. There is a stress function for each material layer, and there are four constants of integration for each stress function; therefore, there are twelve independent constants of integration for which there must be twelve independent boundary conditions to obtain the solution. The stress functions are denoted as  $\phi_1$ ,  $\phi_2$ , and  $\phi_3$ , where the subscripts correspond to the material layers indicated in Figure 1. The constants of integration are denoted as  $C_1^1$ ,  $C_2^1$ , etc., corresponding to  $\phi_1$ ;  $C_1^2$ ,  $C_2^2$ , etc., corresponding to  $\phi_2$ , etc.

The boundary conditions are as follows. The superscripts denote the corresponding material layers as indicated in Figure 1.

$$\tau_{xy}^1(x, -y_1) = 0 \quad (5a)$$

$$\sigma_y^1(x, -y_1) = 0 \quad (5b)$$

$$\tau_{xy}^1(x, 0) = \tau_{xy}^2(x, 0) \quad (5c)$$

$$\sigma_y^1(x, 0) = \sigma_y^2(x, 0) \quad (5d)$$

$$u^1(x, 0) = u^2(x, 0) \quad (5e)$$

$$v^1(x, 0) = v^2(x, 0) \quad (5f)$$

$$\tau_{xy}^2(x, y_2) = \tau_{xy}^3(x, y_2) \quad (5g)$$

$$\sigma_y^2(x, y_2) = \sigma_y^3(x, y_2) \quad (5h)$$

$$u^2(x, y_2) = u^3(x, y_2) \quad (5i)$$

$$v^2(x, y_2) = v^3(x, y_2) \quad (5j)$$

$$\tau_{xy}^3(x, y_3) = 0 \quad (5k)$$

$$\sigma_y^3(x, y_3) = \sum a_n \sin \frac{n\pi x}{L} \quad (5l)$$

$$\int_A \sigma_x(0, y) dy = 0 \quad (6a)$$

$$\int_A \sigma_x(L, y) dy = 0 \quad (6b)$$

$$\int_A \sigma_x(0, y) y dy = 0 \quad (6c)$$

$$\int_A \sigma_x(L, y) y dy = 0 \quad (6d)$$

$$\int_A \tau_{xy}(0, y) dy = \text{reaction} \quad (6e)$$

$$\int_A \tau_{xy}(L, y) dy = \text{reaction} \quad (6f)$$

where the letter A associated with the integral sign denotes the total cross-sectional area of the beam.

Boundary conditions in Eq. 5 are used to evaluate the twelve constants of integration, whereas boundary conditions in Eq. 6 were identically satisfied by the choice of the stress functions. The load in Eq. 5l is represented by a Fourier sin series expansion, thereby allowing a large degree of freedom in the type of loadings that may be studied.

By applying the boundary conditions (Eq. 5), twelve simultaneous linear equations are obtained with the constants of integration as unknowns. The constants of integration are dependent on the parameter  $\alpha$  which in turn depends on the value of the integer  $n$ . For this reason, the twelve equations must generally be solved for each value of  $n$ . The number of times the set of equations must be solved therefore depends on the number of terms of the series used to represent a given loading. Because of the large number of computations involved, numerical results are best obtained with the use of a digital computer.

## DISCUSSION OF RESULTS

The examples of three material beams presented and discussed in this paper have central material layer depths that are small in comparison to the depths of the top and bottom layers. In addition, the total depth of the beam is small in comparison to its length. This type of beam simulates a composite beam consisting of two materials bonded together by a third material. The dimensions and material properties of the top and bottom layers are selected so that the neutral axis of the entire cross-section is located very near the top of the bottom layer.

Except for the depths of the central and top layers, the relative beam dimensions are the same for all the examples presented. In terms of the dimensionless ratio  $x/L$ , the span length is unity. The vertical coordinates and dimensions are expressed in terms of the ratio  $y/L$ . For a given beam, three  $y/L$  values are assigned, one for each material layer. For the examples presented here, the  $y/L$  values for the top and bottom edges are 0.016 and 0.050, respectively. The moduli of elasticity are expressed as ratios of a particular layer to the modulus of elasticity of the bottom layer; hence, the modular ratio of the bottom layer is always unity. The letter  $n$  is used to denote the modular ratios and the subscripts associated with the  $n$ 's identify the associated material layer as shown in Figure 1. The associated subscripts should prevent any

confusion with the integer  $n$  used previously. The modular ratios of the top and central layers are varied; however, Poisson's ratios for all three layers are kept the same throughout this investigation. Poisson's ratios for the top, central, and bottom layers are 0.15, 0.20, and 0.25, respectively. The relative dimensions and material properties were chosen to simulate, as nearly as possible, composite beams used in practice.

For most of the examples presented, a single concentrated load of unity was applied at midspan. In some cases two concentrated loads symmetrically placed about midspan are used. The total magnitude of the loads is unity, and they are located at  $x/L$  equal 0.30 and 0.70. The concentrated loads are approximated by using a uniformly distributed load acting over approximately  $1/100$  of the span length. All beams presented here were symmetrically loaded; however, the solution developed is not limited to symmetrically loaded beams. The solutions obtained are valid in the range of elastic behavior of the materials only.

The horizontal tensile stress  $\sigma$  and the vertical displacement  $v$  are obtained at midspan for simple end-supported beams in which the modular ratio of the top material layer and the modular ratio and depth of the central material layer are varied. The top layer modular ratios  $n_3$  used are 4.0, 6.0, and 8.0. The central layer depth is varied from a  $y/L$  value of 0.0005 to 0.0020 in increments of 0.0005. The central layer modular ratio  $n_2$  is assigned values of 1.0, 0.10, 0.01, 0.005, 0.001, and 0.0001. The horizontal stresses and vertical displacements (or deflections) at midspan of the beams are presented in terms of the ratios  $\sigma/\sigma_e$  and  $\delta/\delta_e$ , where  $\sigma$  and  $\delta$  are obtained from the expressions for  $\sigma_x$  and  $v$  developed earlier and  $\sigma_e$  and  $\delta_e$  are obtained by using the transformed section and the elementary beam formulas (Appendix). The stresses  $\sigma$  and  $\sigma_e$  are the tensile stresses in the lower fiber of the beam. This stress is used because the compressive stresses in the top fibers of the beam are not comparable. The concentrated load is applied at midspan; hence, the elasticity solution yields a local effect in the stresses at midspan, whereas the elementary solution does not. This local effect is not nearly as pronounced in the bottom fibers of the beam. Stress variation along the beam for the stresses in the top and bottom fibers of the beam are shown in Figure 2.

The deflection  $\delta$  was computed at the top edge of the bottom layer ( $y = 0$ ). This would not introduce a significant error because the neutral axis is very near this edge. The deflection  $\delta_e$  was obtained at the neutral axis of the section as computed by elementary methods.

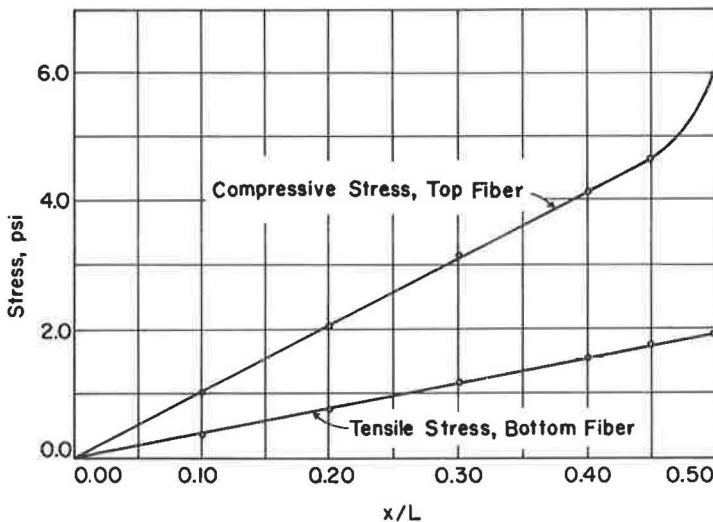


Figure 2. Stress variation along beam's length.

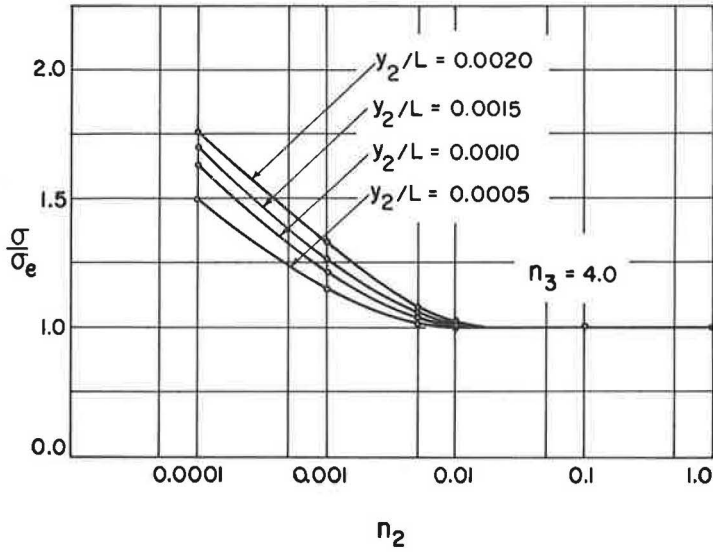


Figure 3. Stress ratio vs central layer modular ratio.

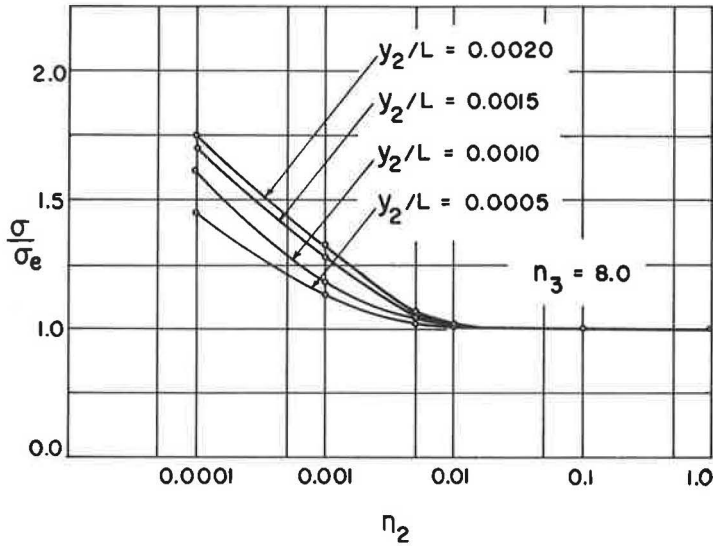


Figure 4. Stress ratio vs central layer modular ratio.

The results of this part of the investigation are shown in Figures 3 through 8 where the stress ratio  $\sigma/\sigma_e$  and the deflection ratio  $\delta/\delta_e$  are plotted against the modular ratio  $n_2$  of the central layer. Figures 3 and 4 show that for central layer modular ratios between 0.01 and 1.0 the stress ratio is very nearly unity. The significance of this is that for this range of  $n_2$  the stresses are predicted with sufficient accuracy by the use of the transformed section and the elementary beam stress formulas. Although evidence is not presented here, this statement holds true for both normal and shearing stresses, and also for any type of loading (8). The homogeneous beam would produce the largest shearing stress, and the shearing stress decreases as the central layer modular ratio decreases; hence, the elementary shear stress formula would yield slightly conservative results in the central modular ratio range listed previously.

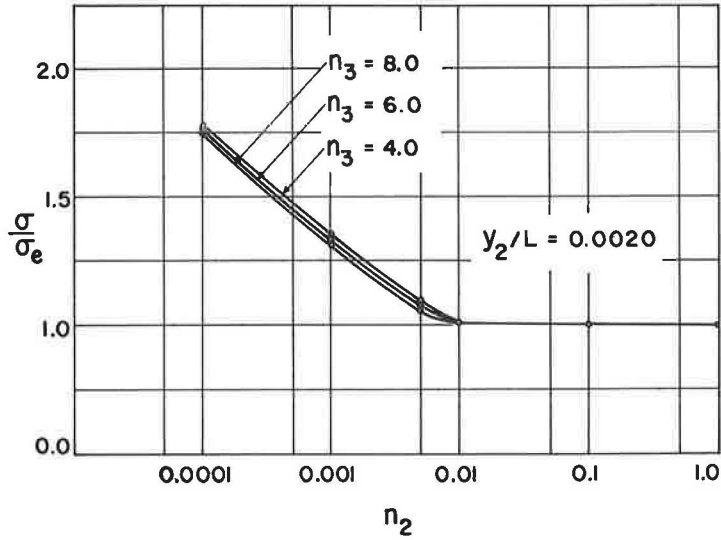


Figure 5. Stress ratio vs central layer modular ratio.

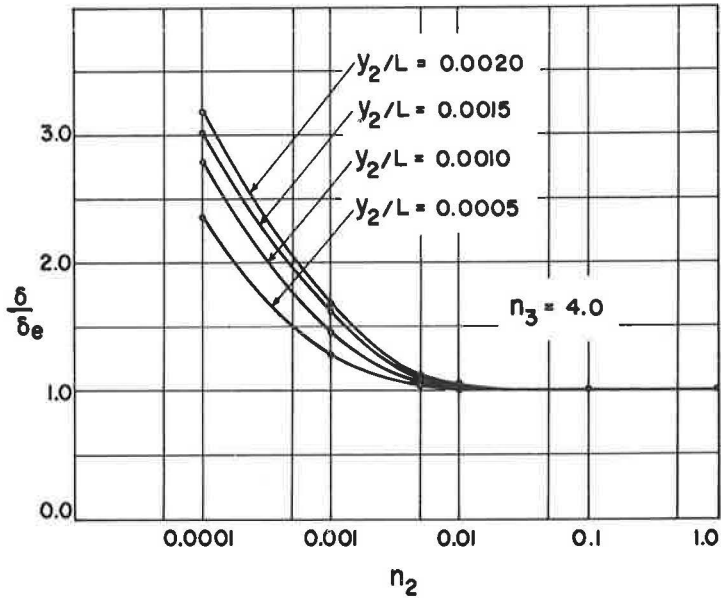


Figure 6. Deflection ratio vs central layer modular ratio.

For modular ratios less than about 0.01, the stress ratios increase; hence, the stresses computed with the elementary stress formulas would be in error, the magnitude of the error increasing as the central layer modular ratio becomes smaller. Figures 3 and 4 show that the central layer depths considered did not have a significant effect on the stress ratios in the range of central layer modular ratios between 0.01 and 1.0. The central layer depths noticeably affected the stress ratios for modular ratios  $n_3$  less than about 0.01. The stresses increase with increasing central layer depths. Figure 5 shows that the stress ratios are not greatly affected by the value of the modular ratio of the top layer within the range of values considered.

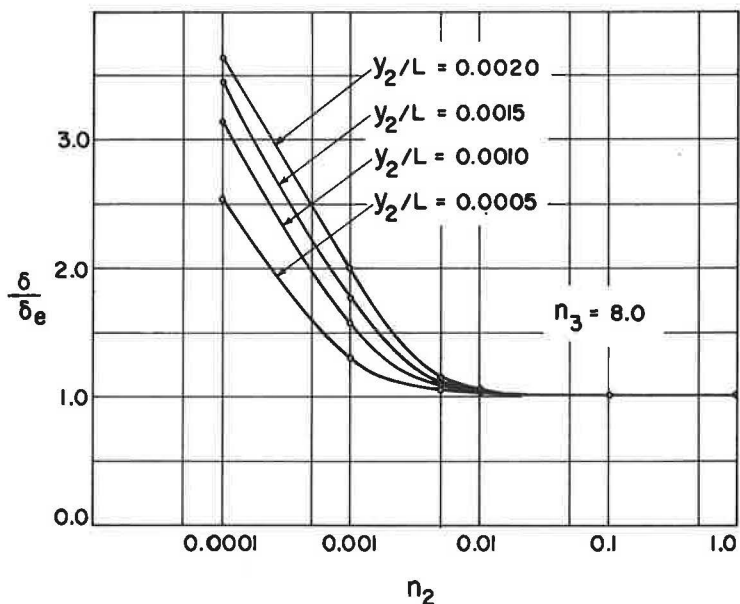


Figure 7. Deflection ratio vs central layer modular ratio.

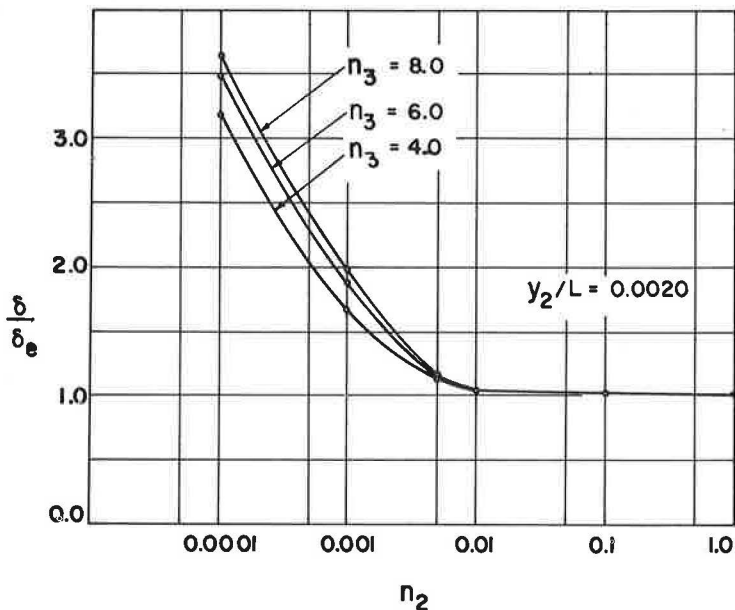


Figure 8. Deflection ratio vs central layer modular ratio.

The deflection ratios vs the central layer modular ratios are shown in Figures 6 and 7. In general, the foregoing discussion on the stress ratios also applies to the deflection ratios. Between the central layer modular ratios of 0.01 to 1.0, the elementary beam formulas for deflection may be used. The deflections are more sensitive to the central layer depths and top layer modular ratios than the stresses for central modular ratios of about 0.01 and less (Fig. 8). The deflection ratios increase as the top layer modular ratios increase.

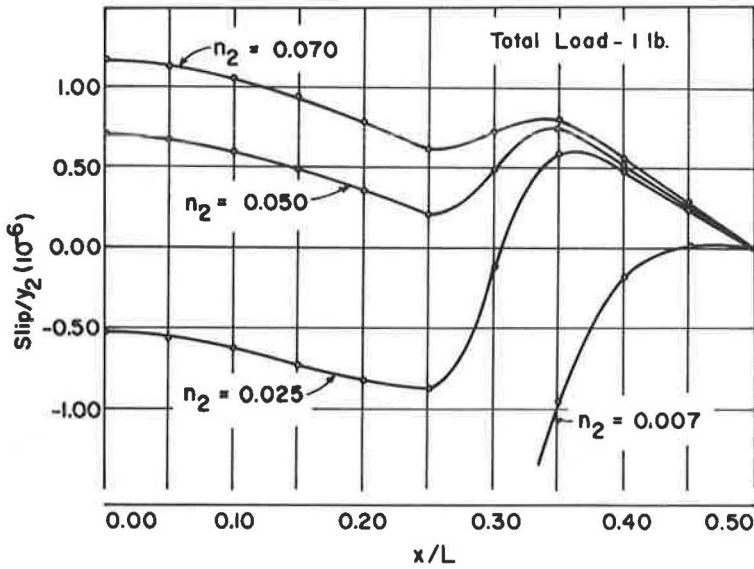


Figure 9. Slip curves for different central layer modular ratios.

The three material or composite beams presented here are considered to satisfy the assumptions on which the mathematical solution is based, i. e., the beams are in a condition of plane stress. Composite beams used in construction do not generally satisfy the assumption of a plane stress condition. Their cross-sections are neither rectangular shaped nor are their widths small in comparison to their depths; hence, the predominate normal stress is not uniformly distributed across the width of the cross-section. Even though T-beams cannot be accurately analyzed, in gaining an adequate insight into the behavior of continuously connected composite beams, the purpose of this investigation has been realized. Another investigation is being conducted to determine a more exact method of analyzing T-beams.

In previous investigations of composite beams (3, 5, 7) the relative displacement at a point between the upper and lower material layers was usually measured. This quantity, commonly referred to as slip, was usually measured at the ends of the beams, but in some cases it was also measured at several points along the span length.

Slip curves were obtained for several cases for the purpose of determining the quantities affecting the slip magnitudes and slip distribution along the span length. Here slip is presented as a ratio of the relative displacement between the top and bottom layers at a point to the depth of the central layer. For this study, the beams were loaded by two concentrated loads symmetrically placed about midspan.

Slip curves for beams having different central layer modular ratios  $n_2$  are shown in Figure 9. The slips decrease algebraically as the central layer modular ratios decrease. The slips are positive (a point on the bottom edge of the top layer displaces to the right of a point on the top edge of the bottom layer) along half of the span for a central layer modular ratio of 0.050 and greater. The slips in the region between the end of the beam and the applied load (at  $x/L = 0.30$ ) were negative for a central layer modular ratio of 0.025 and less. Some of the slips in the region between midspan and the applied load remained positive until the central layer modular ratios became very small. The foregoing discussion applied to the left half of the beam. The signs of the slips in the right half of the beam would be opposite to those in the left half of the beam. Positive slips do occur and have been observed by the authors.

The effect on the slips of changing the reaction locations is also investigated. The reactions are placed at  $x/L$  values of 0.00, 0.025, and 0.050. The applied loads are kept the same distance from the ends of the beams. Slip curves for the three reaction locations for beams loaded by two concentrated loads symmetrically

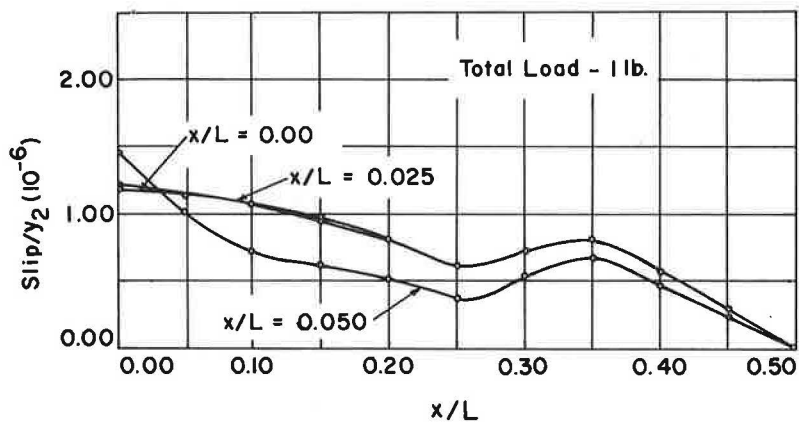


Figure 10. Slip curves for beams with different reaction locations.

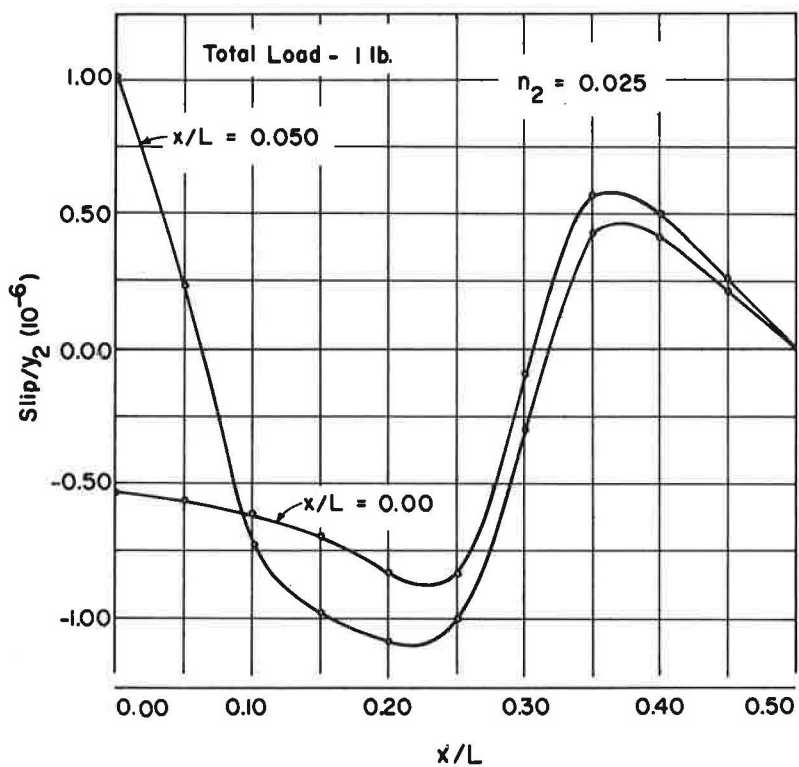


Figure 11. Slip curves for beams with different reaction locations.

placed about midspan are shown in Figure 10. The central modular ratio for the beam is 0.070. The maximum slip, which is positive, occurs at the ends of the beam, and the changing of the reaction location increases the end slips. The end slips increase as the reactions move away from the ends. The effect on the slips is small for the reaction location of  $x/L$  equal to 0.025, but becomes quite pronounced at  $x/L$  equal to 0.050.

Figure 11 shows the slips for the case of the reactions located at the ends were negative between the ends and the applied loads. This beam had a central layer modular ratio of 0.025. For the reaction located at  $x/L$  equal to 0.050, the slip curve had a completely different shape than the curve with the reactions located at the ends. The maximum slip did not occur at the ends. This had been verified by several investigators who performed tests on composite beams (3, 7).

### EXPERIMENTAL TEST RESULTS

A three-layer beam consisting of aluminum, steel, and epoxy resin was constructed, instrumented, and tested for the purpose of showing the effectiveness of the mathematical solution. The test results were then compared to results predicted by the mathematical solution.

Steel and aluminum constituted the top and bottom layers, whereas the epoxy resin constituted the center layer. The cross-sectional dimensions of the steel, aluminum, and epoxy resin were  $\frac{1}{2}$  by  $\frac{1}{2}$  in.,  $\frac{3}{4}$  by  $\frac{1}{2}$  in., and  $\frac{1}{4}$  by  $\frac{1}{2}$  in., respectively. The beam was  $\frac{1}{2}$  in. wide and  $1\frac{1}{2}$  in. deep. The total length of the beam was  $48\frac{1}{2}$  in. During testing the beam was simply supported with a span length of 48 in. The material constants (modulus of elasticity and Poisson's ratio) for the steel and aluminum were taken from a handbook, whereas the material constants for the epoxy resin were obtained by testing tensile specimens. The tensile specimens were molded at the time the beam was constructed, and kept in the same environment as the beam. The strains in the tensile specimens were obtained by means of electric strain gages. The results of the epoxy resin tensile tests are shown in Figure 12. The stress-strain relationship for the epoxy resin was essentially linear.

The model beam was simply supported on knife-edge supports 48 in. apart. The beam was positioned on the supports so that the steel constituted the top layer. Instru-

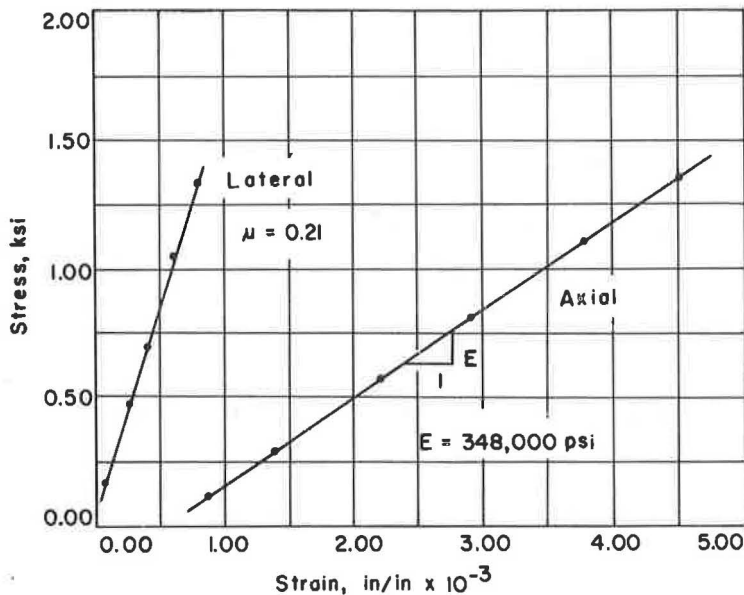


Figure 12. Stress-strain curves for epoxy resin.

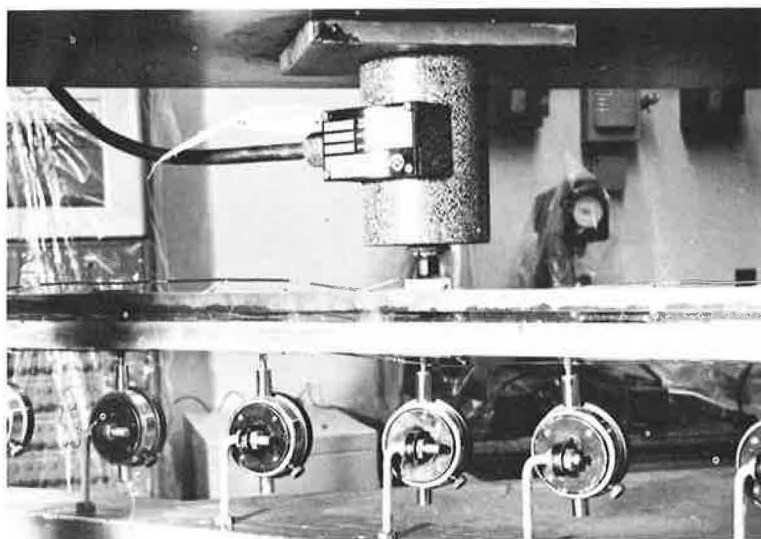


Figure 13. Model beam.

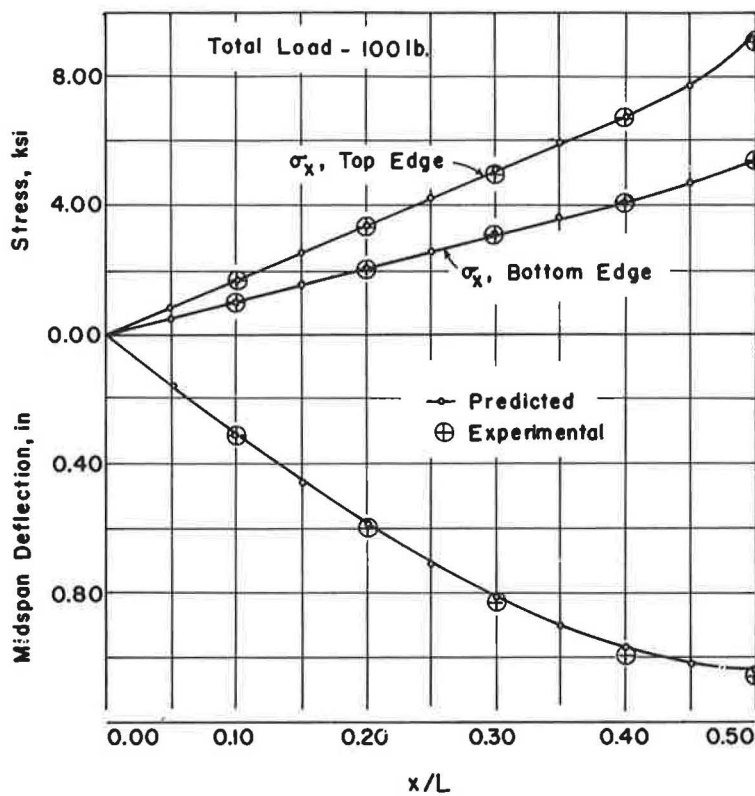


Figure 14. Comparison of predicted and experimental results—single load.

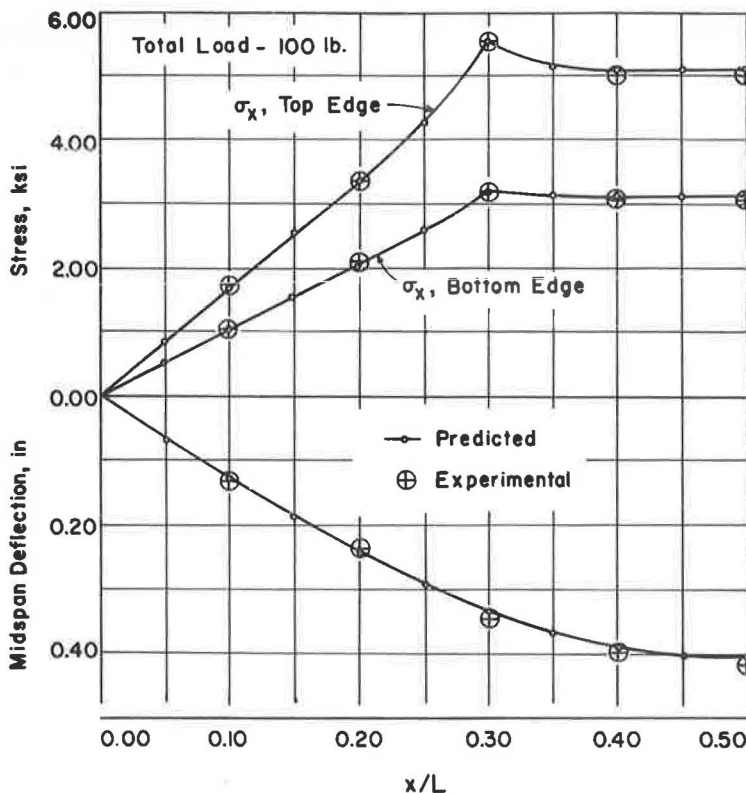


Figure 15. Comparison of predicted and experimental results—two point load.

mentation consisted of electric strain gages and 0.0001-in. dial deflection gages. The electric strain gages were placed on the top and bottom of both the steel and aluminum layers at every one-tenth point of the span (4.8 in. in this case). The dial deflection gages were located at every one-tenth point of the span length. The model beam was not instrumented to measure end slips, because of the lack of sensitive measuring devices. A single concentrated load at midspan and a symmetrically placed two point loading located at  $x/L = 0.30$  and  $0.70$  was used. The load was measured to an accuracy of one pound by means of a load cell. The mathematical solution applied only in the elastic range; hence, during testing the maximum load applied was kept below the yield load. The model beam is shown in Figure 13.

The predicted and experimental horizontal stresses at the top and bottom edges of the model beam for a single concentrated load at midspan and for a symmetrically placed two point loading are shown in Figures 14 and 15, respectively. The values are for a total applied load of 100 lb. There is less than 3 percent difference between the maximum predicted values and the test values.

### CONCLUSIONS

Studies of several examples of three material beams whose central layer depths were small compared to the depths of the other two material layers, and whose total depth was small compared to the beam's length have been presented. For thin central layers, the quantity that had the greatest effect on the predominate stresses and deflections was the central layer modular ratio. It was also shown that for a certain range of central layer modular ratios, the predominate stresses and deflections may be determined with sufficient accuracy by using the transformed section and the elementary formulas for stresses and deflections.

An investigation was conducted to determine the reliability of the relative displacement (slip) at a point between the top and bottom material layers as an indicator of the behavior of composite beams. The slips were sensitive to many factors, and therefore not a reliable indicator for use in experimental studies unless properly interpreted.

A three material model beam was constructed and tested. The test results were compared to results predicted by the mathematical solution. There was little difference between the test values and the predicted values; hence, the effectiveness of the mathematical solution was verified.

The foregoing conclusions are valid in the elastic range of behavior of the materials, and are also subject to the range of the variables considered.

#### REFERENCES

1. Viest, Ivan M. Review of Research on Composite Steel-Concrete Beams. Proc., ASCE, Vol. 86, J. Structural Div., June 1960.
2. Miklofsky, Haaren A., Brown, Martin R., Jr., and Gonsior, Michael, J. Epoxy Bonding Compounds as Shear Connectors in Composite Beams. Rensselaer Polytechnic Inst. Eng. Res. Series RR62-2, Troy, New York, Oct. 1962.
3. Kriegh, James D., and Endebrook, Elton G. The Use of Epoxy Resins in Reinforced Concrete Static Load Tests. Univ. of Arizona Eng. Res. Lab., Tucson, Arizona, Jan. 1963.
4. Stuessi, F. Zusammengesetzte Vollwandtraeger. Publications, Internat. Assoc. for Bridge and Structural Eng., Vol. 8, pp. 249-269, 1947.
5. Jaeger, K. Die Verbundwirkung zwischen Stahltraeger und Stahlbeton platte. Oesterreichischer Ingenieur - Archien (Wien), Vol. 3, No. 4, pp. 295-311, 1949.
6. Newmark, Nathan M., Siess, Chester P., and Viest, Ivan M. Tests and Analysis of Composite Beams with Incomplete Interaction. Proc., Soc. for Experimental Stress Analysis, Vol. 9, No. 1, pp. 75-92, 1951.
7. Hanson, Norman V. Horizontal Shear Connectors. Jour. of the Res. and Dev. Lab., Portland Concrete Assoc., Vol. 2, No. 2, May 1960.
8. Endebrook, Elton G. An Elasticity Solution of the Multi-Material Beam. PhD thesis, Univ. of Arizona, Tucson, Arizona, 1964.

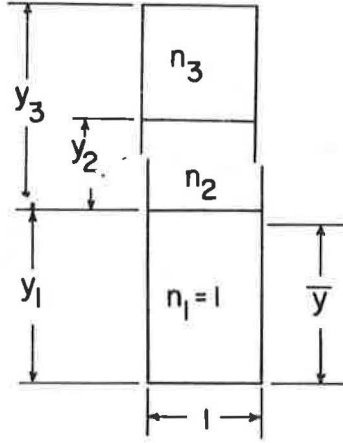
**Appendix****ELEMENTARY METHOD OF COMPUTING STRESSES AND DEFLECTIONS**

Figure 16.

Neutral axis:

$$\bar{y} = \frac{y_1^2/2 + y_2 n_2 (y_2 + y_2/2) + (y_3 - y_2) n_3 \left( y_1 + \frac{y_2 + y_3}{2} \right)}{y_1 + n_2 y_2 + n_3 (y_3 - y_2)}$$

Moment of inertia:

$$I = \frac{1}{12} y_1^3 + y_1 \left( \bar{y} - \frac{y_1}{2} \right)^2 + \frac{1}{12} n_2 y_2^3 + n_2 y_2 \left( y_1 + \frac{y_2}{2} - \bar{y} \right)^2 + \frac{n_3 (y_3 - y_2)^3}{12} + n_3 (y_3 - y_2) \left( y_1 + \frac{y_2 + y_3}{2} - \bar{y} \right)^2$$

Stresses:

$$\sigma_e = \frac{M \bar{y}}{I}$$

Deflections:

$$\delta_e = \frac{PL^3}{48I}$$